




Radiomics as prognostic factor in brain metastases treated with Gamma Knife radiosurgery

Chih-Ying Huang^{1,2} · Cheng-Chia Lee^{2,3,4} · Huai-Che Yang^{2,3} · Chung-Jung Lin^{2,5} · Hsiu-Mei Wu^{2,5} · Wen-Yuh Chung^{2,3} · Cheng-Ying Shiau^{2,6} · Wan-Yuo Guo^{2,5} · David Hung-Chi Pan^{3,7} · Syu-Jyun Peng⁸ 

Received: 13 September 2019 / Accepted: 12 November 2019 / Published online: 4 February 2020
© Springer Science+Business Media, LLC, part of Springer Nature 2019

Abstract

Purpose Gamma Knife radiosurgery (GKRS) is a non-invasive procedure for the treatment of brain metastases. This study sought to determine whether radiomic features of brain metastases derived from pre-GKRS magnetic resonance imaging (MRI) could be used in conjunction with clinical variables to predict the effectiveness of GKRS in achieving local tumor control.

Methods We retrospectively analyzed 161 patients with non-small cell lung cancer (576 brain metastases) who underwent GKRS for brain metastases. The database included clinical data and pre-GKRS MRI. Brain metastases were demarcated by experienced neurosurgeons, and radiomic features of each brain metastasis were extracted. Consensus clustering was used for feature selection. Cox proportional hazards models and cause-specific proportional hazards models were used to correlate clinical variables and radiomic features with local control of brain metastases after GKRS.

Results Multivariate Cox proportional hazards model revealed that higher zone percentage (hazard ratio, HR 0.712; $P = .022$) was independently associated with superior local tumor control. Similarly, multivariate cause-specific proportional hazards model revealed that higher zone percentage (HR 0.699; $P = .014$) was independently associated with superior local tumor control.

Conclusions The zone percentage of brain metastases, a radiomic feature derived from pre-GKRS contrast-enhanced T1-weighted MRIs, was found to be an independent prognostic factor of local tumor control following GKRS in patients with non-small cell lung cancer and brain metastases. Radiomic features indicate the biological basis and characteristics of tumors and could potentially be used as surrogate biomarkers for predicting tumor prognosis following GKRS.

Keywords Radiomics · Gamma knife radiosurgery · Brain metastasis · Magnetic resonance imaging · Prognosis

Electronic supplementary material The online version of this article (<https://doi.org/10.1007/s11060-019-03343-4>) contains supplementary material, which is available to authorized users.

✉ Syu-Jyun Peng
sjpeng2019@tmu.edu.tw

- 1 Department of Medical Education, Taipei Veterans General Hospital, Taipei, Taiwan
- 2 School of Medicine, National Yang-Ming University, Taipei, Taiwan
- 3 Department of Neurosurgery, Neurological Institute, Taipei Veterans General Hospital, Taipei, Taiwan
- 4 Brain Research Center, National Yang-Ming University, Taipei, Taiwan

Introduction

Brain metastases (BMs) are the most frequent malignant intracranial tumors, and the most common primary origin is lung cancer [1, 2]. Non-small cell lung cancer (NSCLC)

- 5 Department of Radiology, Taipei Veterans General Hospital, Taipei, Taiwan
- 6 Cancer Center, Taipei Veterans General Hospital, Taipei, Taiwan
- 7 Department of Neurosurgery, Shuang Ho Hospital, Taipei Medical University, Taipei, Taiwan
- 8 Professional Master Program in Artificial Intelligence in Medicine, College of Medicine, Taipei Medical University, Taipei, Taiwan

constitutes approximately 80% of all lung cancers, and 25–50% of patients with metastatic NSCLCs are affected by BMs during the course of their disease [3, 4]. BMs remain a leading cause of morbidity and mortality despite advances in systemic therapy and improved survival rates for patients with advanced NSCLC. The mean survival of patients with untreated BMs is 1–3 months [5].

Gamma Knife radiosurgery (GKRS) is a promising, non-invasive procedure for the management of BMs. The primary objective of GKRS is local tumor control [6–9]. However, new or recurrent BMs develop in approximately 25–50% of patients within the first 6–12 months after GKRS [10–13]. Several clinical factors are related to local control of BMs after GKRS, including tumor volume [14, 15] and epidermal growth factor receptor (EGFR) mutation status [16, 17]; however, relatively few studies have focused on the correlation between pre-GKRS imaging traits and local tumor control.

Radiomics is a field of study in which image analysis is used to extract quantitative features from medical images. Radiomics has been proposed as a means to explore correlations between imaging traits and clinical outcomes. [18–20]. Radiomic features provide valuable information pertaining to tumor phenotype and microenvironment,

which can be used for tumor classification, prognosis prediction, and treatment response prediction for various cancers, such as BM, lung cancer, head and neck cancer, and glioblastoma multiforme [21–23].

Our objective in this study was to identify radiomic features of BMs derived from pre-GKRS magnetic resonance imaging (MRI) as well as the clinical variables that correlate with local tumor control following GKRS.

Methods

Patients

This retrospective review was based on clinical data and MRI of patients with BMs who underwent GKRS at Taipei Veterans General Hospital between 2012 and 2017. Our research protocol was approved and monitored by the Taipei Veterans General Hospital Institutional Review Board (IRB, IRB number: 2017-09-010BC). A total of 161 patients satisfied the following criteria: (1) Diagnosis with NSCLC confirmed by lung biopsy or open surgery; (2) Diagnosis of one or more BMs confirmed by MRI

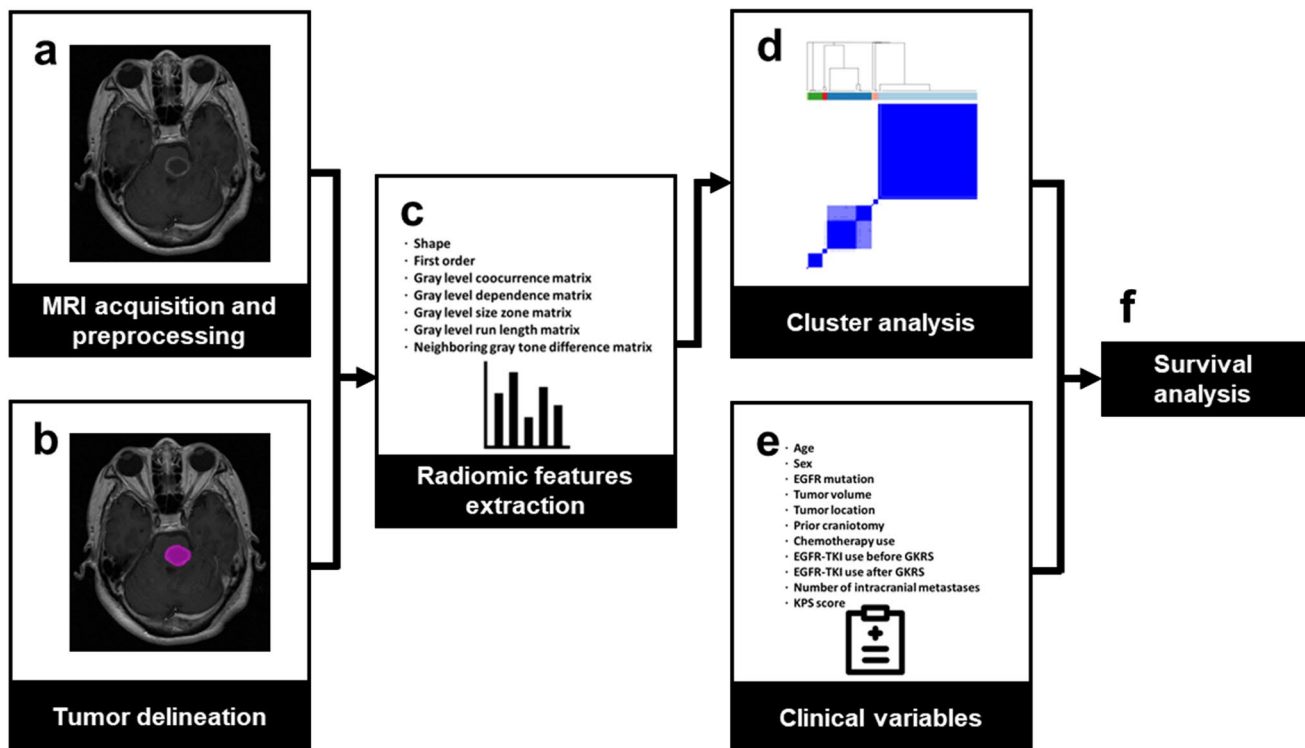


Fig. 1 Analytic pipeline. **a** Axial contrast-enhanced T1-weighted pre-GKRS MRI used in analysis. Preprocessing included skull stripping and Z-score intensity normalization. **b** Tumor regions of interest (ROIs), as demarcated by experienced neurosurgeons. **c** A total of 107 radiomic features were extracted from ROIs using the open-

source software Pyradiomics. **d** Consensus clustering was performed for feature selection. **e** Clinical variables were also used for further analysis. **f** Survival analysis of progression-free survival of tumors was performed using the Cox proportional hazards models and cause-specific proportional hazards models

without brainstem BMs; (3) Treatment with GKRS and no treatment with whole brain radiotherapy (WBRT); (4) At least one clinical and neuroimaging follow-up. The subsequent analytic pipeline was summarized in Fig. 1.

GKRS procedures

GKRS procedures were performed using the Leksell Gamma Unit Model 4C or the Perfexion stereotactic radiosurgery device (Elekta AB, Stockholm, Sweden). The techniques employed at our institution have been detailed in previous papers [24–28]. Following stereotactic Leksell frame placement under monitored anesthesia, all patients underwent pre-GKRS MRI. Dose planning was performed using Gamma Plan software. All GKRS treatment parameters were recorded, including margin and maximum dose.

Radiation dose scheme

We adopted the methods proposed by the Radiation Therapy Oncology Group (RTOG) and the Japanese study group guidelines for the determination of dose schemes. For patients who underwent GKRS in conjunction with WBRT, we followed the dose planning guidelines of RTOG 95-08 [29]: WBRT dose was 37.5 Gy in 15 fractions, and GKRS boost dose was adjusted according to lesion size (24 Gy, 18 Gy, and 15 Gy for BMs measuring < 20 mm, 20–30 mm, and 30–40 mm, respectively). In accordance with the guidelines proposed by Aoyama [30], GKRS dose was (1) varied according to the size of the lesion (22–25 Gy for BMs measuring < 20 mm, 18–20 Gy for BMs measuring > 20 mm) and (2) reduced by 30% in cases where WBRT was administered. In accordance with the guidelines provided by RTOG 90-05 [31] pertaining to GKRS use in the treatment of recurrent, previously irradiated BMs, we evaluated doses in terms of maximum BM diameter: 18 Gy for BMs measuring \leq 20 mm, 15 Gy for BMs measuring 21–30 mm, and 12 Gy for BMs measuring 31–40 mm.

MRI acquisition

All pre-GKRS MRI data were collected using a Signa HDxt 1.5 T (GE healthcare Milwaukee, WI) scanner with an eight-channel phased-array neurovascular coil to obtain images. Pre-GKRS contrast-enhanced T1-weighted images were used for analysis. The parameters used to acquire contrast-enhanced T1-weighted spin-echo images were as follows: repetition time (TR) = 450–666.668 ms, echo time (TE) = 8–9 ms, field of view (FOV) = 258.85–261.06 mm, number of excitations (NEX) = 2, slice thickness = 3 mm, and pixel spacing = 0.5 mm.

Radiomic feature extraction

Tumor regions of interest (ROIs) were demarcated manually by experienced neurosurgeons (CC Lee and HC Yang). Preprocessing, including skull stripping and Z-score intensity normalization, was performed using Statistical Parametric Mapping 12 (SPM12, Wellcome Department of Cognitive Neurology, London, UK, <https://www.fil.ion.ucl.ac.uk/spm/>) and Python (version 3.6.7). Feature extraction was performed on all tumor ROIs using the PyRadiomics package (version 2.0.1) with resampling of all images to $1 \times 1 \times 1 \text{ mm}^3$ [32]. A total of 107 radiomic features were obtained (using a bin size of 25), including 14 shape features, 18 first order features, and 75 texture features, such as gray level co-occurrence matrix (GLCM), gray level dependence matrix (GLDM), gray level run length matrix (GLRLM), gray level size zone matrix (GLSZM), and neighboring gray tone difference matrix (NGTDM) features (Supplementary Table 1). All features were extracted in 3D and converted to Z-scores for normalization.

Consensus clustering

Feature selection was performed to reduce redundancy in extracted radiomic features [20, 33]. This was achieved using consensus clustering, which is a methodology based on resampling [22, 34, 35]. An appropriate number of clusters was selected from delta area plots. For each cluster, we obtained the medoid, which is the representative feature with highest average pairwise correlation within a cluster. The medoids, which represent the clusters they belong to, were regarded as potential promising radiomic signatures and were used as independent variables in subsequent statistical analyses. Using the R package ConsensusClusterPlus (v 1.46.0) [36], consensus clustering was performed using hierarchical clustering and a dissimilarity measure based on Pearson correlation ($1 - r$), with 80% item resampling and 1000 resampling iterations.

Outcomes and follow-ups

Follow-up neuroimaging (including contrast-enhanced, thin-sliced MRIs of the whole brain) and clinical evaluations (including symptoms related to chemotherapy/target therapy) were performed at 3-month intervals. Note that neuroimaging studies were independently reviewed by experienced neurosurgeons. Tumor response was assessed by comparing follow-up MRIs to pre-GKRS MRIs. The results were categorized as follows: (1) regression (> 10% decrease in tumor volume); (2) stable (< 10% increase or

Table 1 Clinical characteristics of 576 brain metastatic tumors in 161 NSCLC patients

Characteristic	Medians or frequencies	Ranges or percentages	IQRs for continuous variables
Per patient (n = 161)			
Age (y/o)	61.50	29.17–89.17	52.36–69.74
Sex (male: female)	65:96	40.37:59.63%	
Number of intracranial metastases			
1	47	29.19%	
2	36	22.36%	
3	19	11.80%	
> 3	59	36.65%	
Extracranial metastases	68	42.24%	
KPS score	90	60–100	90–90
Neurological deficits			
Long tract signs	25	15.53%	
Cerebellar signs	10	6.21%	
Cranial nerve palsy	20	12.42%	
High cortical dysfunction	3	1.86%	
Asymptomatic	112	69.57%	
Image follow-up (months)	12.7	0.4–63.8	6.1–21.2
Clinical follow-up (months)	10.5	0.0–64.7	5.8–22.6
Prior craniotomy	9	5.59%	
Chemotherapy use	88	54.66%	
EGFR-TKI use before GKRS	101	62.73%	
EGFR-TKI use after GKRS	120	74.53%	
Tumor histology			
Pure adenocarcinoma	158	98.14%	
Squamous cell carcinoma	1	0.62%	
Adenocarcinoma + Squamous cell carcinoma	1	0.62%	
Adenocarcinoma + Large cell carcinoma	1	0.62%	
EGFR mutation type			
No mutation	44	27.33%	
L858R point mutation	48	29.81%	
Exon 19 deletion	40	24.84%	
G719X point mutation	3	1.86%	
Exon 21 point mutation	2	1.24%	
Exon 20 insertion	2	1.24%	
T790M point mutation	1	0.62%	
S768I point mutation	1	0.62%	
Inconclusive	4	2.48%	
Combined mutations			
L858R and T790M	10	6.21%	
Exon 19 deletion and T790M	5	3.11%	
L858R and S768I	1	0.62%	
Survival (months)	14.7	0.7–64.7	9.2–25.0
Per tumor (n = 576)			
Tumor volume (mL)	0.14	0.02–32.43	0.07–0.52
Location of tumor			
Frontal lobe	191	33.16%	
Parietal lobe	97	16.84%	
Temporal lobe	81	14.06%	
Occipital lobe	79	13.72%	

Table 1 (continued)

Characteristic	Medians or frequencies	Ranges or percentages	IQRs for continuous variables
Insula	15	2.60%	
Basal ganglia and thalamus	25	4.34%	
Cerebellum	88	15.28%	
SRS protocol			
Margin dose (Gy)	20.0	12.0–30.0	18.0–21.0
Maximum dose (Gy)	30.0	20.0–50.0	26.9–32.7
Isodose level (%)	65.5	50.0–95.0	60.0–78.3

EGFR epidermal growth factor receptor, *GKRS* Gamma knife radiosurgery, *Gy* gray, *IQR* interquartile range, *KPS* Karnofsky Performance Scale, *TKI* tyrosine-kinase inhibitor, *y/o* years old

decrease in tumor volume); and (3) progression (> 10% increase in tumor volume). Local tumor control included stable tumor responses and/or tumor regression [17, 37].

Statistical analysis

Descriptive statistics for continuous variables were reported as medians, ranges and interquartile ranges (IQRs). Categorical variables were reported as frequencies and percentages. Progression-free survival (PFS) was defined as the time from GKRS to tumor progression. Survival analysis of PFS (i.e., local tumor control) was assessed using Cox proportional hazards models and cause-specific proportional hazards models [38, 39], due to the presence of mortality as the competing risk, to identify potential prognostic factors. Variables that were found to be significant at the 0.10 level in univariate analyses were entered into multivariate models. Statistical significance was defined as $P < 0.05$. All statistical analyses were performed using SPSS (version 24, IBM Corporation, Armonk, NY) and the R package survival (v. 2.44-1.1) [40, 41].

Results

Patient characteristics

This study investigated a series of 161 patients treated with GKRS with a total of 576 BMs. Patient characteristics, tumor characteristics, and GKRS data are summarized in Table 1.

The patient cohort comprised 65 males and 96 females. Median patient age was 61.50 years (range: 29.17–89.17 years, IQR: 52.36–69.74 years), and median Karnofsky Performance Scale (KPS) score was 90 (range: 60–100, IQR: 90–90). A total of 158 patients were diagnosed with pure adenocarcinoma, while 1 patient had squamous cell carcinoma, 1 patient had mixed adenocarcinoma and squamous cell carcinoma, and 1 patient had mixed

adenocarcinoma and large cell carcinoma. With regard to EGFR mutation status, 44 patients had wild-type EGFR (no mutations), whereas the other patients had EGFR mutations, most of which comprised L858R point mutations, followed by Exon 19 deletion mutations. Most patients were asymptomatic; however, 25 patients presented with long tract signs, 10 patients presented with cerebellar signs, 20 patients had cranial nerve palsy, and 3 patients showed high cortical dysfunction. In addition, 47, 36, 19, and 59 patients respectively had 1, 2, 3, and > 3 intracranial metastases, and 68 patients had extracranial metastases. Prior to GKRS, 9 patients had undergone a craniotomy. Furthermore, 88 patients underwent chemotherapy, and 101 and 120 patients respectively used EGFR-tyrosine kinase inhibitors (EGFR-TKIs) before and after GKRS. The median lengths of neuroimaging and clinical follow-ups were 12.7 months (range: 0.4–63.8 months, IQR: 6.1–21.2 months) and 10.5 months (range: 0.0–64.7 months, IQR: 5.8–22.6 months), respectively, and median survival was 14.7 months (range: 0.7–64.7 months, IQR: 9.2–25.0 months).

The median tumor volume of BMs was 0.14 mL (range: 0.02–32.43 mL, IQR: 0.07–0.52 mL). The locations of the 576 BMs were as follows: frontal lobe (191), parietal lobe (97), temporal lobe (81), occipital lobe (79), insula (15), basal ganglia and thalamus (25), and cerebellum (88). The median margin dose was 20.0 Gy (range: 12.0–30.0 Gy, IQR: 18.0–21.0 Gy), and the median maximal dose was 30.0 Gy (range: 20.0–50.0 Gy, IQR: 26.9–32.7 Gy).

Clustering

Consensus clustering resulted in 8 distinct radiomic feature clusters, based on the delta area plot (Supplementary Fig. 1) (size: 1 to 62 features per cluster). Details regarding cluster size, associated radiomic features, and the medoids of each cluster are provided in Supplementary Table 2.

Table 2 Prognostic factors associated with local tumor progression (derived using Cox proportional hazards models)

Factors	Univariate			Multivariate		
	<i>p</i> value	HR	95% CI	<i>p</i> value	HR	95% CI
Clinical variables						
Age	0.430	0.992	0.972–1.012			
Sex (female vs. male)	0.159	0.706	0.435–1.145			
EGFR mutation	+0.059	0.586	0.336–1.021	+0.095	0.618	0.351–1.087
Tumor volume	**0.004	1.000	1.000–1.000	0.365	1.000	1.000–1.000
Tumor location (infratentorial vs. supratentorial)	0.285	1.407	0.752–2.633			
Prior craniotomy	*0.044	2.386	1.023–5.567	0.135	1.930	0.816–4.569
Chemotherapy use	0.203	0.726	0.443–1.189			
EGFR-TKI use before GKRS	0.131	0.687	0.422–1.119			
EGFR-TKI use after GKRS	0.431	0.767	0.397–1.483			
Number of intracranial metastases	+0.072	0.947	0.893–1.005	0.342	0.970	0.911–1.033
KPS score	0.622	1.008	0.977–1.039			
Radiomic features						
original_shape_Elongation	0.137	1.216	0.939–1.575			
original_firstorder_Mean	0.258	1.135	0.912–1.413			
original_shape_Sphericity	0.785	1.033	0.818–1.305			
original_glszm_LowGrayLevelZoneEmphasis	+0.068	0.757	0.562–1.021	0.305	0.859	0.643–1.148
original_firstorder_Minimum	0.584	0.938	0.744–1.181			
original_firstorder_Kurtosis	0.425	1.091	0.881–1.352			
original_glcm_Id	0.473	1.091	0.861–1.382			
original_glszm_ZonePercentage	**0.005	0.673	0.510–0.888	*0.022	0.712	0.533–0.951

CI confidence interval, EGFR epidermal growth factor receptor, GKRS Gamma Knife radiosurgery, HR hazard ratio, KPS Karnofsky Performance Scale, TKI tyrosine-kinase inhibitor

+*p* < 0.1, **p* < 0.05, ***p* < 0.01, ****p* < 0.001

Prognostic factors associated with local tumor progression using Cox proportional hazards models

Variables that proved significant at the 0.10 level in univariate Cox proportional hazards models were considered potential prognostic factors and were entered into a multivariate Cox proportional hazards model.

In univariate Cox proportional hazards models, among clinical variables, positive EGFR mutation (hazard ratio, HR 0.586; *P* = 0.059) and number of intracranial metastases (HR 0.947; *P* = 0.072) were associated with a better tumor control, while tumor volume (HR 1.000; *P* = 0.004) and prior craniotomy (HR 2.386; *P* = 0.044) were associated with a poorer tumor control. Among radiomic features, higher low gray level zone emphasis (original_glszm_LowGrayLevelZoneEmphasis) (HR 0.757; *P* = 0.068) and higher zone percentage (original_glszm_ZonePercentage) (HR 0.673; *P* = 0.005) of BMs were associated with a better tumor control in univariate Cox proportional hazards models. These variables were thus input into a multivariate Cox proportional hazards model.

The multivariate Cox proportional hazards model revealed that higher zone percentage (HR 0.712;

P = 0.022) was independently associated with the favorable local control of BMs.

Univariate and multivariate Cox proportional hazards models pertaining to the local control of BMs are summarized in Table 2.

Prognostic factors associated with local tumor progression using cause-specific proportional hazards models

Since patients' survival in our cohort was relatively short, cause-specific proportional hazards models were also performed due to the presence of mortality as the competing risk. Variables that proved significant at the 0.10 level in univariate cause-specific proportional hazards models were considered potential prognostic factors and were entered into a multivariate cause-specific proportional hazards model.

In univariate cause-specific proportional hazards models, among clinical variables, female sex (HR 0.664; *P* = 0.096) and number of intracranial metastases (HR 0.928; *P* = 0.009) were associated with a better tumor control, while tumor

Table 3 Prognostic factors associated with local tumor progression (derived using cause-specific proportional hazards models)

Factors	Univariate			Multivariate		
	<i>p</i> value	HR	95% CI	<i>p</i> value	HR	95% CI
Clinical variables						
Age	0.648	0.995	0.976–1.015			
Sex (female vs. male)	+0.096	0.664	0.410–1.076	0.362	0.793	0.482–1.306
EGFR mutation	0.166	0.677	0.389–1.176			
Tumor volume	**0.001	1.000	1.000–1.000	0.382	1.000	1.000–1.000
Tumor location (infratentorial vs. supratentorial)	0.386	1.319	0.706–2.464			
Prior craniotomy	*0.047	2.355	1.013–5.476	0.160	1.861	0.783–4.422
Chemotherapy use	0.454	0.830	0.509–1.352			
EGFR-TKI use before GKRS	0.713	0.884	0.458–1.705			
EGFR-TKI use after GKRS	0.388	0.808	0.499–1.310			
Number of intracranial metastases	**0.009	0.928	0.877–0.981	0.128	0.954	0.897–1.014
KPS score	0.219	1.020	0.989–1.052			
Radiomic features						
original_shape_Elongation	0.133	1.217	0.942–1.573			
original_firstorder_Mean	0.184	1.162	0.932–1.448			
original_shape_Sphericity	0.978	0.997	0.796–1.249			
original_glszm_LowGrayLevelZoneEmphasis	*0.030	0.716	0.529–0.968	0.349	0.870	0.650–1.165
original_firstorder_Minimum	0.420	0.909	0.721–1.146			
original_firstorder_Kurtosis	0.450	1.082	0.883–1.325			
original_glcm_Id	0.407	1.101	0.877–1.384			
original_glszm_ZonePercentage	**0.002	0.648	0.495–0.848	*0.014	0.699	0.526–0.929

CI confidence interval, EGFR epidermal growth factor receptor, GKRS Gamma Knife radiosurgery, HR hazard ratio, KPS Karnofsky Performance Scale, TKI tyrosine-kinase inhibitor

+ $p < 0.1$, * $p < 0.05$, ** $p < 0.01$, *** $p < 0.001$

volume (HR 1.000; $P = 0.001$) and prior craniotomy (HR 2.355 $P = 0.047$) were associated with a poorer tumor control. Among radiomic features, higher low gray level zone emphasis (HR 0.716; $P = 0.030$) and higher zone percentage (HR 0.648; $P = 0.002$) of BMs were associated with a better tumor control in univariate cause-specific proportional hazards models. These variables were thus input into a multivariate cause-specific proportional hazards model.

The multivariate cause-specific proportional hazards model revealed that higher zone percentage (HR 0.699; $P = 0.014$) was independently associated with the favorable local control of BMs.

Univariate and multivariate cause-specific proportional hazards models pertaining to the local control of BMs are summarized in Table 3.

Case illustration

Zone percentage is a means of measuring the coarseness of texture by taking the ratio of the number of zones and the number of voxels in the tumor. A higher zone percentage indicates that a larger proportion of the tumor comprises

small zones and that the tumor has a finer texture. In contrast-enhanced T1-weighted MR images, a higher zone percentage indicates that the enhancement pattern of the tumor is more homogeneous. In this study, we observed that there was a higher likelihood of local tumor control following GKRS in NSCLC-BMs with higher zone percentages. Tumors with lower zone percentages are coarser, which means that their enhancement patterns are more heterogeneous, suggestive of punctate-, nodular-, or ring-enhancing patterns. We observed that there was a lower likelihood of local tumor control (following GKRS) in NSCLC-BMs with lower zone percentages. Overall, these findings suggest that radiomic features could potentially be used as prognosis factors for local tumor control.

One example of NSCLC-BMs with a lower zone percentage is described in the following: A 51-year-old female presented with lung adenocarcinoma (EGFR mutation (–)) and BMs. One BM was found at the left frontal lobe. Due to the ring-enhancement pattern of this BM in contrast-enhanced T1-weighted MRI prior to GKRS, it can be inferred that its zone percentage was low (0.226, Z-score = –1.246). Based on low zone percentage of this BM, it is unlikely that this BM would respond favorably to GKRS. After undergoing

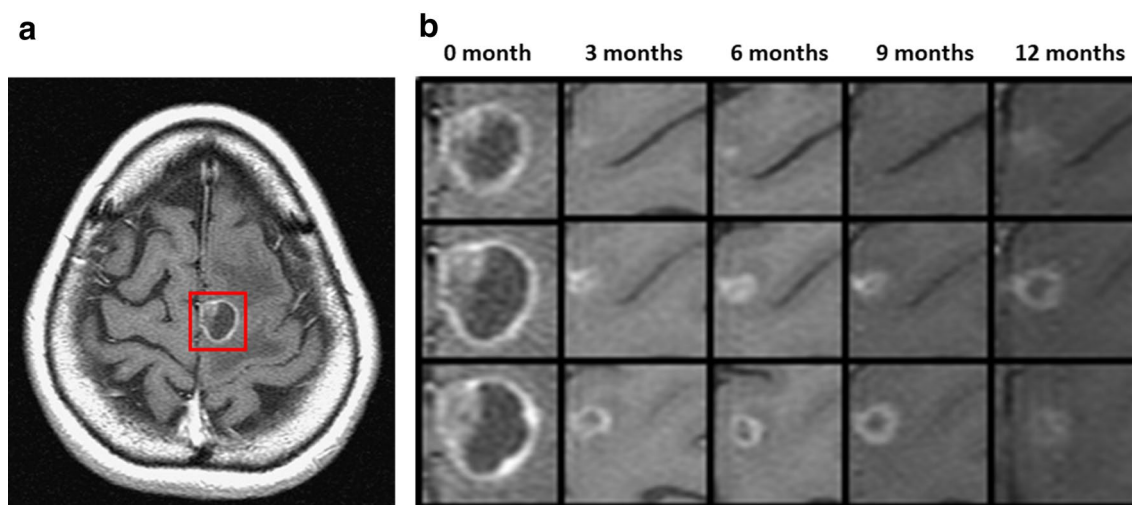


Fig. 2 Example case 1. A 51-year-old female with lung adenocarcinoma (EGFR mutation (-)) and BMs treated with GKRS. **a** Axial contrast-enhanced T1-weighted MRI of one of the BMs prior to GKRS, zone percentage=0.226 (Z-score=-1.246). **b** Three con-

secutive axial slices of contrast-enhanced T1-weighted MRI of the tumor prior to GKRS and at 3, 6, 9, and 12 months after GKRS (left to right). Tumor progression was diagnosed at 9 months after GKRS

GKRS, this patient received regular follow-ups that included an MRI every 3 months. At 9 months after GKRS, tumor progression was diagnosed, thereby confirming our prediction (Fig. 2).

Another example is described in the following: A 76-year-old female presented with lung adenocarcinoma (EGFR mutation (+), Exon 19 deletions) and BMs, one of which was found at the right thalamus. Given the homogeneous enhancement pattern associated with this BM, we can infer that its zone percentage was high (0.440, Z-score=0.407). Based on high zone percentage of this BM, it is likely that this BM would respond favorably to GKRS. This patient received regular follow-ups that included an MRI every 3 months. At 18 months after GKRS, this BM was still under control (Fig. 3).

Discussion

This study investigated relationships between radiomic features and the prognosis of NSCLC-BMs after GKRS. For this, we applied consensus clustering to 107 quantitative radiomic features extracted from MRI scans of 576 NSCLC-BMs, and then selected the medoids for survival analysis. Our results indicated that, after adjusting for important clinical variables, NSCLC-BMs with a higher zone percentage were more likely to respond favorably to GKRS (local tumor control).

Other features in the cluster associated with the zone percentage are also highly correlated to it (Supplementary

Table 2). For example, the feature referred to as ‘short run emphasis’ (original_glrIm_ShortRunEmphasis) indicates the distribution of short run lengths, where a greater value indicates a finer texture. Another feature referred to as ‘small area emphasis’ (original_glszm_SmallAreaEmphasis) indicates the distribution of small size zones, where a greater value indicates a finer texture. We found that these features could perhaps be used as prognostic factors for local tumor control in NSCLC-BM patients following GKRS; however, we selected zone percentage as the medoid in subsequent analyses because this feature showed the highest average pairwise correlation within this cluster.

Previous studies on the prognosis of BM patients treated with GKRS have identified several clinical prognostic factors for local tumor control, including tumor volume [14, 15] and EGFR mutation status [16, 17]. Although relatively little research has focused on the correlation between pre-GKRS imaging traits and local tumor control, one study revealed that baseline homogeneous enhancement patterns correlated with local tumor control in BM patients following GKRS [42]. This finding is consistent with our results. However, our study employed a radiomic approach, which is a more quantitative and objective way to describe enhancement patterns. Another study showed that tumor necrosis in pre-treatment contrast-enhanced MR or computed tomography images was a prognostic factor for survival in BM patients treated using GKRS, but was not predictive of local control [43]. Those authors claimed that the lack of an association between necrosis and local control might be due to statistical anomalies. That study failed to provide evidence supporting

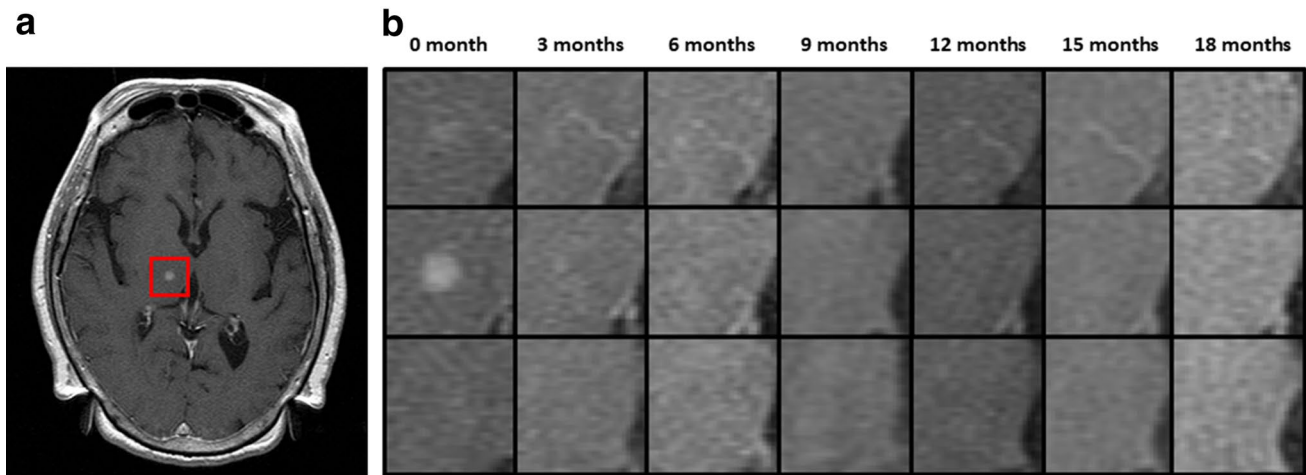


Fig. 3 Example case 2. A 76-year-old female with lung adenocarcinoma (EGFR mutation (+), Exon 19 deletions) and BMs treated with GKRS. **a** Axial contrast-enhanced T1-weighted MRI of one of the BMs prior to GKRS, zone percentage=0.440 (Z-score=0.407).

b Three consecutive axial slices contrast-enhanced T1-weighted MRI of the tumor prior to GKRS and at 3, 6, 9, 12, 15, and 18 months after GKRS (left to right). No tumor progression was found

an association between necrosis and local tumor control; however, our results provide evidence to support the assertion because zone percentage could be used to measure the degree of necrosis in tumors.

Radiomic features of tumors provide information related to their underlying pathophysiology, microenvironment, phenotype, and even genotype [18–20]. Our results revealed that zone percentage and other related radiomic features are associated with local tumor control of NSCLC-BMs following GKRS. This implies that there may be fundamental phenotypic or genotypic differences among BMs with different value of these radiomic features. One possible explanation may be related to the effect of hypoxia on radiosensitivity. Specifically, necrosis results in hypoxia, which reduces radiosensitivity and is associated with poorer local tumor control after radiotherapy or radiosurgery [44]. This hypothesis is supported by findings from several studies on head and neck tumors [45, 46]. The link between zone percentage and the level of tumor necrosis suggests that zone percentage could potentially be used as a surrogate marker for tumor prognosis following radiotherapy or radiosurgery, including GKRS.

This study had several limitations. Firstly, it was subject to the inherent shortcomings of the retrospective study design. For example, this study was subject to selection bias, as the decision to initiate GKRS treatment was made at the discretion of physicians and patients. Besides, MRI protocols were not standardized for every patient. Furthermore, because this study was based on patients in a single center, an external validation cohort is required to further confirm our results. Finally, only contrast-enhanced T1-weighted images were used in this study. Therefore, additional

analyses to identify links between other MRI sequences and clinical outcomes should be pursued.

Conclusions

This study demonstrated that the zone percentage of BMs, a radiomic feature derived from pre-GKRS contrast-enhanced T1-weighted MRIs, was found to be an independent prognostic factor of local tumor control following GKRS in NSCLC-BM patients. Radiomic features indicate the biological basis and characteristics of tumors and could potentially be used as surrogate biomarkers for predicting tumor prognosis following GKRS.

Acknowledgements The authors would like to thank all colleagues who contributed to this study. We are grateful to our research assistants, Fong-Jiao Lee, Hsueh-Jen Huang, Wen-Chi Ku, Yi-Bei Tseng, and Jr Lan Huang for their data recording and transcription. We thank the editor and series editor for constructive criticisms of an earlier version of this article. This work was financially supported in part by the Ministry of Science and Technology, Taiwan, under the project MOST 108-2221-E-038-019 and the project MOST 108-2634-F-010-002, in part by the Research Grants for Newly Hired Faculty by the Taipei Medical University in Taiwan, under the project TMU 108-AE1-B04, and in part by the Brain Research Center, National Yang-Ming University from The Featured Areas Research Center Program within the framework of the Higher Education Sprout Project by the Ministry of Education (MOE) in Taiwan.

Compliance with ethical standards

Conflict of interest All authors declare that they have no conflicts of interest.

References

- Kaal ECA, Niël CGJH, Vecht CJ (2005) Therapeutic management of brain metastasis. *Lancet Neurol* 4:289–298. [https://doi.org/10.1016/s1474-4422\(05\)70072-7](https://doi.org/10.1016/s1474-4422(05)70072-7)
- Schouten LJ, Rutten J, Huveneers HA, Twijnstra A (2002) Incidence of brain metastases in a cohort of patients with carcinoma of the breast, colon, kidney, and lung and melanoma. *Cancer* 94:2698–2705. <https://doi.org/10.1002/cncr.10541>
- Schuette W (2004) Treatment of brain metastases from lung cancer: chemotherapy. *Lung Cancer* 45:S253–S257
- Sørensen J, Hansen H, Hansen M, Dombernowsky P (1988) Brain metastases in adenocarcinoma of the lung: frequency, risk groups, and prognosis. *J Clin Oncol* 6:1474–1480
- Ali A, Goffin JR, Arnold A, Ellis PM (2013) Survival of patients with non-small-cell lung cancer after a diagnosis of brain metastases. *Curr Oncol*. <https://doi.org/10.3747/co.20.1481>
- Hussain A, Brown PD, Stafford SL, Pollock BE (2007) Stereotactic radiosurgery for brainstem metastases: Survival, tumor control, and patient outcomes. *Int J Radiat Oncol Biol Phys* 67:521–524. <https://doi.org/10.1016/j.ijrobp.2006.08.081>
- Trifiletti DM, Lee C-C, Kano H, Cohen J, Janopaul-Naylor J, Alonso-Basanta M, Lee JYK, Simonova G, Liscak R, Wolf A, Kvint S, Grills IS, Johnson M, Liu K-D, Lin C-J, Mathieu D, Héroux F, Silva D, Sharma M, Cifarelli CP, Watson CN, Hack JD, Goffin JR, Kondziolka D, Barnett G, Lunsford LD, Sheehan JP (2016) Stereotactic radiosurgery for brainstem metastases: an international cooperative study to define response and toxicity. *Int J Radiat Oncol Biol Phys* 96:280–288. <https://doi.org/10.1016/j.ijrobp.2016.06.009>
- Jawahar A, Matthew RE, Minagar A, Shukla D, Zhang JH, Willis BK, Ampil F, Nanda A (2004) Gamma knife surgery in the management of brain metastases from lung carcinoma: a retrospective analysis of survival, local tumor control, and freedom from new brain metastasis. *J Neurosurg* 100:842–847
- Petrovich ZYC, Giannotta SL, O'Day S, Apuzzo ML (2002) Survival and pattern of failure in brain metastasis treated with stereotactic gamma knife radiosurgery. *J Neurosurg* 97(Supplement 5):499–506
- Ayala-Peacock DN, Peiffer AM, Lucas JT, Isom S, Kuremsky JG, Urbanic JJ, Bourland JD, Laxton AW, Tatter SB, Shaw EG, Chan MD (2014) A nomogram for predicting distant brain failure in patients treated with gamma knife stereotactic radiosurgery without whole brain radiotherapy. *Neuro Oncol* 16:1283–1288. <https://doi.org/10.1093/neuonc/nou018>
- Zindler JD, Slotman BJ, Lagerwaard FJ (2014) Patterns of distant brain recurrences after radiosurgery alone for newly diagnosed brain metastases: Implications for salvage therapy. *Radiother Oncol* 112:212–216. <https://doi.org/10.1016/j.radonc.2014.07.007>
- Gorovets D, Ayala-Peacock D, Tybor DJ, Rava P, Ebner D, Cielo D, Noren G, Wazer DE, Chan M, Hepel JT (2017) Multi-institutional nomogram predicting survival free from salvage whole brain radiation after radiosurgery in patients with brain metastases. *Int J Radiat Oncol Biol Phys* 97:246–253. <https://doi.org/10.1016/j.ijrobp.2016.09.043>
- McTyre E, Ayala-Peacock D, Contessa J, Corso C, Chiang V, Chung C, Fiveash J, Ahluwalia M, Kotecha R, Chao S, Attia A, Henson A, Hepel J, Braunstein S, Chan M (2018) Multi-institutional competing risks analysis of distant brain failure and salvage patterns after upfront radiosurgery without whole brain radiotherapy for brain metastasis. *Ann Oncol* 29:497–503. <https://doi.org/10.1093/annonc/mdx740>
- Baschnagel AM, Meyer KD, Chen PY, Krauss DJ, Olson RE, Pieper DR, Maitz AH, Ye H, Grills IS (2013) Tumor volume as a predictor of survival and local control in patients with brain metastases treated with Gamma Knife surgery. *J Neurosurg* 119:1139–1144. <https://doi.org/10.3171/2013.7.JNS13431>
- Kim DG, Chung HT, Gwak HS, Paek SH, Jung HW, Han DH. (2000) Gamma knife radiosurgery for brain metastases: prognostic factors for survival and local control. *J Neurosurg* 93(supplement_3): 23–29
- Lee H-L, Chung T-S, Ting L-L, Tsai J-T, Chen S-W, Chiou J-F, Leung HW-C, Liu HE (2012) EGFR mutations are associated with favorable intracranial response and progression-free survival following brain irradiation in non-small cell lung cancer patients with brain metastases. *Radiat Oncol* 7:181
- Lee C-C, Hsu SP, Lin C-J, Wu H-M, Chen Y-W, Luo Y-H, Chiang C-L, Hu Y-S, Chung W-Y, Shiao C-Y (2019) Epidermal growth factor receptor mutations: association with favorable local tumor control following Gamma Knife radiosurgery in patients with non-small cell lung cancer and brain metastases. *J Neurosurg* 1:1–8
- Kumar V, Gu Y, Basu S, Berglund A, Eschrich SA, Schabath MB, Forster K, Aerts HJ, Dekker A, Fenstermacher D, Goldgof DB, Hall LO, Lambin P, Balagurunathan Y, Gatenby RA, Gillies RJ (2012) Radiomics: the process and the challenges. *Magn Reson Imaging* 30:1234–1248. <https://doi.org/10.1016/j.mri.2012.06.010>
- Lambin P, Rios-Velazquez E, Leijenaar R, Carvalho S, van Stiphout RG, Granton P, Zegers CM, Gillies R, Boellard R, Dekker A, Aerts HJ (2012) Radiomics: extracting more information from medical images using advanced feature analysis. *Eur J Cancer* 48:441–446. <https://doi.org/10.1016/j.ejca.2011.11.036>
- Gillies RJ, Kinahan PE, Hricak H (2015) Radiomics: images are more than pictures, they are data. *Radiology* 278:563–577
- Aerts HJ, Velazquez ER, Leijenaar RT, Parmar C, Grossmann P, Carvalho S, Bussink J, Monshouwer R, Haibe-Kains B, Rietveld D, Hoebers F, Rietbergen MM, Leemans CR, Dekker A, Quackenbush J, Gillies RJ, Lambin P (2014) Decoding tumour phenotype by noninvasive imaging using a quantitative radiomics approach. *Nat Commun* 5:4006. <https://doi.org/10.1038/ncomms5006>
- Li Z-C, Li Q-H, Song B-L, Chen Y-S, Sun Q-C, Xie Y-Q, Wang L (2016) Clustering of MRI radiomics features for glioblastoma multiforme: an initial study. *International Conference on Medical Imaging and Augmented Reality*. Springer, Berlin, pp 311–319
- Kniep HC, Madesta F, Schneider T, Hanning U, Schonfeld MH, Schon G, Fiehler J, Gauer T, Werner R, Gellissen S (2019) Radiomics of brain MRI: utility in prediction of metastatic tumor type. *Radiology* 290:479–487. <https://doi.org/10.1148/radiol.2018180946>
- Lee C-C, Chou C-L, Chen C-J, Yang H-C, Wu H-M, Shiao C-Y, Pan DH-C, Chung W-Y (2018) Stereotactic radiosurgery for hypervascular intracranial tumors. *J Neuro Oncol* 140:547–558. <https://doi.org/10.1007/s11060-018-2980-8>
- Lee CC, Pan DH, Chung WY, Liu KD, Yang HC, Wu HM, Guo WY, Shih YH (2012) Brainstem cavernous malformations: the role of Gamma Knife surgery. *J Neurosurg*. <https://doi.org/10.3171/2012.8.GKS121066>
- Lee CC, Wintermark M, Xu Z, Yen CP, Schlesinger D, Sheehan JP (2014) Application of diffusion-weighted magnetic resonance imaging to predict the intracranial metastatic tumor response to gamma knife radiosurgery. *J Neurooncol* 118:351–361. <https://doi.org/10.1007/s11060-014-1439-9>
- Lee CC, Yen CP, Xu Z, Schlesinger D, Sheehan J (2014) Large intracranial metastatic tumors treated by Gamma Knife surgery: outcomes and prognostic factors. *J Neurosurg* 120:52–59. <https://doi.org/10.3171/2013.9.JNS131163>
- Pai FY, Chen CJ, Wang WH, Yang HC, Lin CJ, Wu HM, Lin YC, Chen HS, Yen YS, Chung WY, Guo WY, Pan DH, Shiao CY, Lee CC (2019) Low-dose Gamma Knife radiosurgery for acromegaly. *Neurosurgery* 85:E20–E30. <https://doi.org/10.1093/neuros/nyy410>

29. Andrews DW, Scott CB, Sperduto PW, Flanders AE, Gaspar LE, Schell MC, Werner-Wasik M, Demas W, Ryu J, Bahary J-P, Souhami L, Rotman M, Mehta MP, Curran WJ (2004) Whole brain radiation therapy with or without stereotactic radiosurgery boost for patients with one to three brain metastases: phase III results of the RTOG 9508 randomised trial. *Lancet* 363:1665–1672. [https://doi.org/10.1016/s0140-6736\(04\)16250-8](https://doi.org/10.1016/s0140-6736(04)16250-8)
30. Aoyama H, Shirato H, Tago M, Nakagawa K, Toyoda T, Hatano K, Kenjo M, Oya N, Hirota S, Shioura H (2006) Stereotactic radiosurgery plus whole-brain radiation therapy vs stereotactic radiosurgery alone for treatment of brain metastases: a randomized controlled trial. *JAMA* 295:2483–2491
31. Shaw E, Scott C, Souhami L, Dinapoli R, Kline R, Loeffler J, Farnan N (2000) Single dose radiosurgical treatment of recurrent previously irradiated primary brain tumors and brain metastases: final report of RTOG protocol 90–05. *International J Radiat Oncol Biol Phys* 47:291–298
32. van Griethuysen JJM, Fedorov A, Parmar C, Hosny A, Aucoin N, Narayan V, Beets-Tan RGH, Fillion-Robin JC, Pieper S, Aerts H (2017) Computational radiomics system to decode the radiographic phenotype. *Cancer Res* 77:e104–e107. <https://doi.org/10.1158/0008-5472.CAN-17-0339>
33. Rizzo S, Botta F, Raimondi S, Origgi D, Fanciullo C, Morganti AG, Bellomi M (2018) Radiomics: the facts and the challenges of image analysis. *Eur Radiol Exp* 2:36. <https://doi.org/10.1186/s41747-018-0068-z>
34. Parmar C, Leijenaar RT, Grossmann P, Rios Velazquez E, Bussink J, Rietveld D, Rietbergen MM, Haibe-Kains B, Lambin P, Aerts HJ (2015) Radiomic feature clusters and prognostic signatures specific for Lung and Head & Neck cancer. *Sci Rep* 5:11044. <https://doi.org/10.1038/srep11044>
35. Braman NM, Etesami M, Prasanna P, Dubchuk C, Gilmore H, Tiwari P, Plecha D, Madabhushi A (2017) Intratumoral and peritumoral radiomics for the pretreatment prediction of pathological complete response to neoadjuvant chemotherapy based on breast DCE-MRI. *Breast Cancer Res.* <https://doi.org/10.1186/s13058-017-0846-1>
36. Monti S, Tamayo P, Mesirov J, Golub T (2003) Consensus clustering: a resampling-based method for class discovery and visualization of gene expression microarray data. *Mach Learn* 52:91–118
37. Snell JW, Sheehan J, Stroila M, Steiner L (2006) Assessment of imaging studies used with radiosurgery: a volumetric algorithm and an estimation of its error. *J Neurosurg* 104:157–162
38. Dignam JJ, Zhang Q, Kocherginsky M (2012) The use and interpretation of competing risks regression models. *Clin Cancer Res* 18:2301–2308
39. Noordzij M, Leffondré K, van Stralen KJ, Zoccali C, Dekker FW, Jager KJ (2013) When do we need competing risks methods for survival analysis in nephrology? *Nephrol Dial Transplant* 28:2670–2677
40. Zhang Z (2017) Survival analysis in the presence of competing risks. *Ann Transl Med* 5(3):47
41. Therneau TM, Grambsch PM (2013) Modeling survival data: extending the Cox model. Springer Science & Business Media, Berlin
42. Peterson AM, Meltzer CC, Evanson EJ, Flickinger JC, Kondziolka D (1999) MR imaging response of brain metastases after gamma knife stereotactic radiosurgery. *Radiology* 211:807–814
43. Martens K, Meyners T, Rades D, Tronnier V, Bonsanto MM, Petersen D, Dunst J, Dellas K (2013) The prognostic value of tumor necrosis in patients undergoing stereotactic radiosurgery of brain metastases. *Radiat Oncol* 8:162
44. Rockwell S, Dobrucki IT, Kim EY, Marrison ST, Vu VT (2009) Hypoxia and radiation therapy: past history, ongoing research, and future promise. *Curr Mol Med* 9:442–458
45. Kuhnt T, Mueller A-C, Pelz T, Haensgen G, Bloching M, Koesling S, Schubert J, Dunst J (2005) Impact of tumor control and presence of visible necrosis in head and neck cancer patients treated with radiotherapy or radiochemotherapy. *J Cancer Res Clin Oncol* 131:758–764
46. Stadler P, Becker A, Feldmann HJ, Hänsen G, Dunst J, Würschmidt F, Molls M (1999) Influence of the hypoxic subvolume on the survival of patients with head and neck cancer. *Int J Radiat Oncol Biol Phys* 44:749–754

Publisher's Note Springer Nature remains neutral with regard to jurisdictional claims in published maps and institutional affiliations.